Supporting Information

Pohjoismäki et al. 10.1073/pnas.1303046110

SI Results and Discussion

Mitochondrial Biogenesis in *Sod2*$^{+/-}$ Hearts. Both *Sod2*$^{+/-}$ and *Sod2*$^{+/-}$;*Tw*$^{+}$ mouse hearts showed a significant up-regulation of *Ppar*s, *Ppargc*s (PGC-1s), as well as *Hif1a* (Fig. S5*E*), which control nuclear encoded mitochondrial genes (1). PGC-1α is known to be activated by ROS (2), whereas *Hif1a* and *Pparg* are transcriptional targets of the mTOR pathway (3). *Sod2*$^{+/-}$;*Tw*$^{+}$ hearts showed a significant decrease in key components of the mitochondrial oxidative phosphorylation (OXPHOS) machinery and of components of the β-oxidation pathway despite up-regulation of factors that normally drive mitochondrial biogenesis (Fig. S5 *F–H*). The decrease in mitochondrial OXPHOS components and β-oxidation pathway most likely indicates compromised mitochondrial function, whereas down-regulation of the monoamine oxidase *Maoa*, as well as the up-regulation of antioxidant defense genes including *Sod3*, *Cat* (catalase), and the remaining superoxide dismutase 2 (*Sod2*) allele (Fig. S5*D*) seem to reflect compensatory adaptations to reduce the ROS load. This adaptation is in accordance with the elevated levels of p53 in *Sod2*$^{+/-}$ and *Sod2*$^{+/-}$;*Tw*$^{+}$ mice, an important regulator of antioxidant defenses (4). Notably, also PGC-1α (*Ppargc1a*; Fig. S5) is required for induction of antioxidant defenses besides its role in mitochondrial biogenesis (2).

SI Materials and Methods

Southern Hybridization. Probes for Southern hybridization were designed as follows (nucleotide coordinates indicated in the probe names: F, forward; R, reverse).

Mouse mtDNA (GenBank accession no. NC_005089.1) probes for copy number and ClaI 2D-agarose gel electrophoresis (2D-AGE):

Mm14783F -AGATGCAGATAAAATTCCATTTCAC

Mm 15333R -CATTTCAGGTTTACAAGACCAGAGT

Mouse 18S gene (GenBank accession no. NR_003278.3) probes:

18S-851F: CCGCAGCTAGGAATAATGGA

18S-1347R: AACTAAGAACGGCCATGCAC

Deep Sequencing Analysis. Enriched mtDNA was extracted from crude mitochondrial fractions of hearts by differential centrifugation. Sequencing libraries were prepared by using the Illumina TruSeq kit according to the manufacturer's instructions. Samples were multiplexed, and paired-end sequencing of all samples was carried out in a single lane of an Illumina HiSEq. 2000 sequencer with data processing by using CASAVA 1.7. All subsequent steps were carried out by using CLCBio Genomics Workbench. Reads were trimmed by using default quality parameters and a minimum length cutoff of 60 bp and assembled against NC_005089.1 at low stringency (cutoff 0.5 read length at 0.8 similarity), extracted, and then assembled again at high stringency (0.95 length, 0.9 similarity). Reads that assembled at low stringency were used for local BLAST searches with a word length of 15 to identify chimeric reads indicative of recombination by using cluster coordinates. High stringency assemblies were used for single-nucleotide variant (SNV) detection by using a quality cutoff of Q30 for central base and average Q25 for an 11-bp neighborhood window. SNV frequencies were calculated per base as pass filter counts/pass filter coverage and then average frequencies per base determined from this value inclusive of positions with zero SNV calls. Data were controlled for the presence of nuclear-encoded mtDNA pseudogenes (5). It should be also noted that cardiomyocytes are postmitotic, and nuclear DNA in general has a much lower mutation rate compared with mtDNA. Therefore, the contribution of few copies of nuclear DNA (nDNA) pseudogenes to the de novo mutation rate is marginal compared with thousands of copies of mtDNA. However, being nonfunctional, nDNA mitochondrial pseudogenes accumulate mutations over generations. If present in significant amounts in mtDNA preparations, these mutations should show up as common polymorphisms shared by siblings. However, common polymorphisms were not observed in our dataset (Fig. S1), where only few mutations shared by siblings were present, most likely representing low-level (<1%) mtDNA heteroplasmy and originating from maternal germ line. In contrast, inherited pseudogene would light up in the mutation rank data as a consistent pattern of common polymorphisms.

Human Samples and the Analysis of Recombined Heart mtDNA. The heart mtDNA recombination analysis was performed by using heart mtDNA from a patient suffering from Kearn Sayre Syndrome (KSS). The sample was obtained by the Newcastle University with a written consent of the family (6, 7). KSS is caused by high levels of heteroplasmic 4-kb common deletion of mtDNA. Aged-matched healthy controls were obtained from forensic autopsies at the University of Tampere as part of the Tampere Coronary Study, approved by the Ethics Committee of Tampere University Hospital (DNO 1239/32/200/01) and the Finnish National Authority for Medico-legal Affairs. For more details, see Pohjoismäki et al (6).

Adult human hearts contain significant amounts of dimeric circular mtDNA (8). If these dimers are formed via recombination, KSS patients should have recombinants between deleted and wild-type mtDNA molecules. Because the KSS deletion removes a number of restriction sites, the recombinants can be distinguished by size differences. Restriction digest, 1D-, and long–2D-AGE analysis were performed as described (8). Southern hybridization was performed by using a probe for nucleotides 35–611.

Cytochrome Oxidase and Succinate Dehydrogenase Stain. Frozen heart muscle samples were embedded and sectioned as described in *Materials and Methods*. Cytochrome oxidase (COX) stain (5 mg of 3,3′-diaminobenzidine tetrahydrochloride, 20 μg of catalase, and 10 mg of cytochrome *c* in 10 mL of 30 mM NaH_2PO_4 at pH 7.4) was added on the unfixed tissue sections on glass slides and incubated for 30 min in a humidity chamber at 37 °C. The COX stain was carefully removed, and succinate dehydrogenase (SDH) counter stain (2.5 mg/mL nitroblue tetrazolium, 30 mM NaH_2PO_4, and 1 mM K-EGTA at pH 7.4) was added on the samples and incubated for an additional 1 h in a humidity chamber at 37 °C. After staining, the tissue sections were dehydrated in an ethanol series of 70%, 95%, and 100% for 4 min each, followed by three successive baths of xylene each for 4 min. Cover glasses were fixed on object trays by using Entellan Neu (Merck) mounting medium.

1. Goffart S, von Kleist-Retzow JC, Wiesner RJ (2004) Regulation of mitochondrial proliferation in the heart: Power-plant failure contributes to cardiac failure in hypertrophy. *Cardiovasc Res* 64(2):198–207.
2. St-Pierre J, et al. (2006) Suppression of reactive oxygen species and neurodegeneration by the PGC-1 transcriptional coactivators. *Cell* 127(2):397–408.
3. Blagosklonny MV (2008) Aging: ROS or TOR. *Cell Cycle* 7(21):3344–3354.
4. Sablina AA, et al. (2005) The antioxidant function of the p53 tumor suppressor. *Nat Med* 11(12):1306–1313.
5. Williams SL, et al. (2010) The mtDNA mutation spectrum of the progeroid Polg mutator mouse includes abundant control region multimers. *Cell Metab* 12(6):675–682.
6. Pohjoismäki JL, et al. (2010) Developmental and pathological changes in the human cardiac muscle mitochondrial DNA organization, replication and copy number. *PLoS ONE* 5(5):e10426.
7. Lax NZ, et al. (2012) Loss of myelin-associated glycoprotein in kearns-sayre syndrome. *Arch Neurol* 69(4):490–499.
8. Pohjoismäki JL, et al. (2009) Human heart mitochondrial DNA is organized in complex catenated networks containing abundant four-way junctions and replication forks. *J Biol Chem* 284(32):21446–21457.

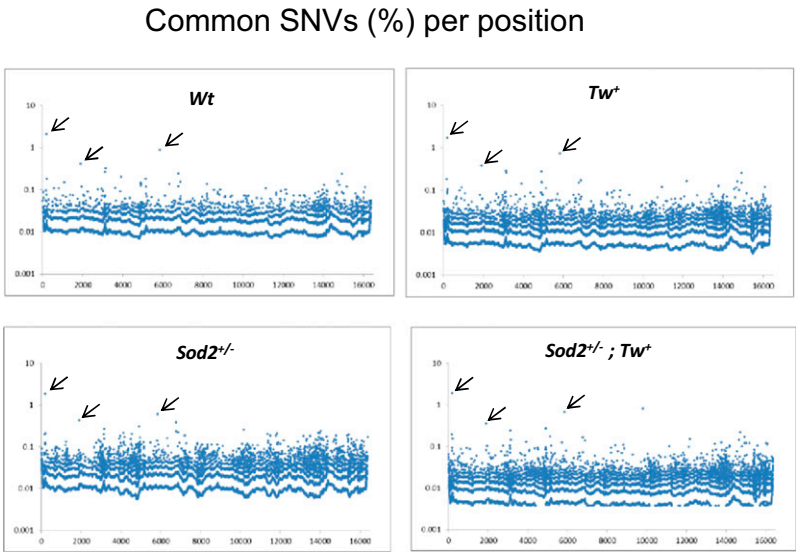

Fig. S1. The analysis of mtDNA sequences demonstrates low-level heteroplasmy. Percentages of the most common SNV at each nucleotide location of mouse mtDNA among littermates of different transgenic backgrounds are shown. The arrows indicate SNVs shared by littermates most likely representing inherited low-level heteroplasmy. Other SNVs represent somatic de novo mutations.

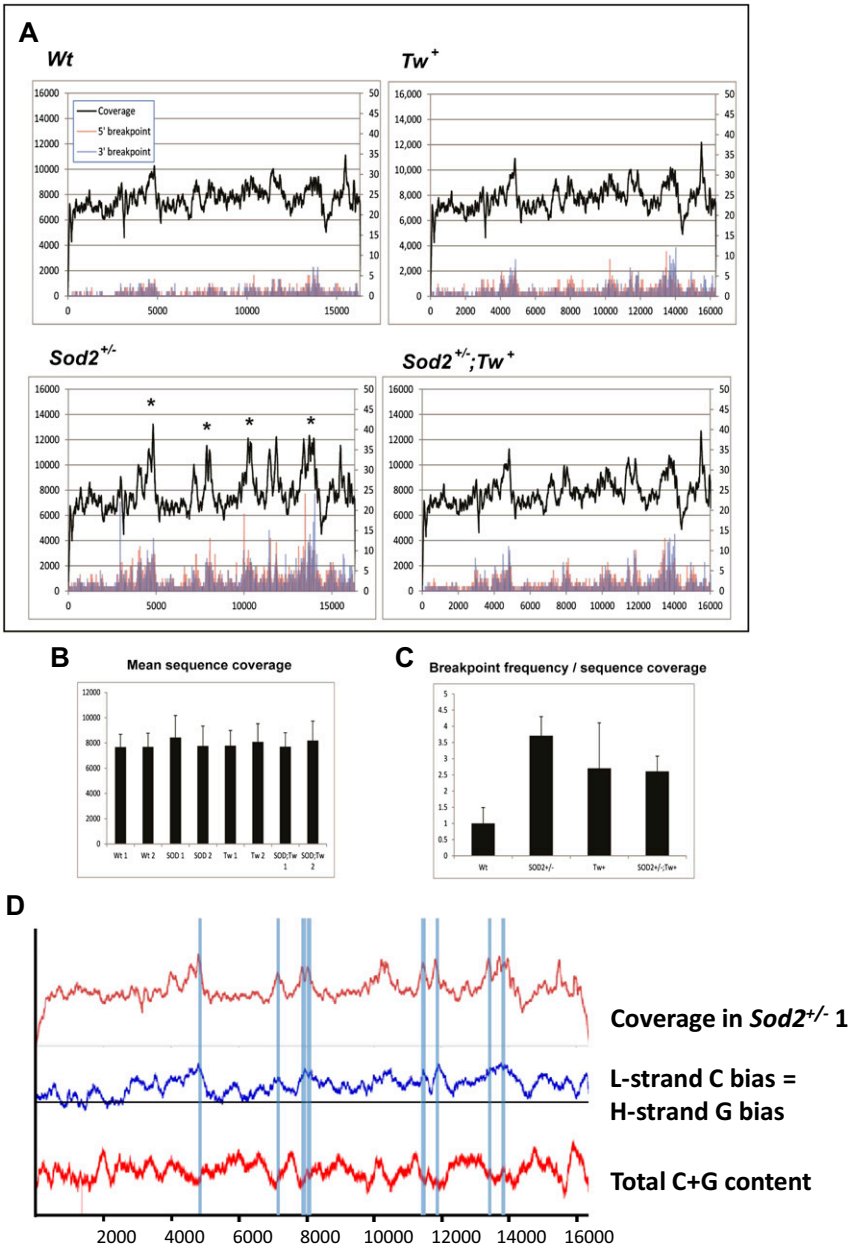

Fig. S2. *Sod2*$^{+/-}$ mouse hearts show an increased rate of mtDNA rearrangements. (*A*) Sequence coverage and rearrangement breakpoints in the mouse heart mtDNA. Sequence coverage (black line) indicates how many times (*y* axis) each mtDNA base (*x* axis coordinates) was sequenced. The frequency of 5′- (red) and 3′-ends (blue) of recombined molecules is given on the right *y* axis in actual counts. Please note the increased coverage (*) of regions carrying the most frequent breakpoints in *Sod2*$^{+/-}$ mouse heart mtDNA. Twinkle overexpression normalized coverage of these peaks to levels of *Tw*$^{+}$ mice. (*B*) No significant difference in the relative overall sequence coverage of heart mtDNAs was observed. (*C*) Relative frequencies of sequence breakpoints normalized to sequence coverage. Elevated rearrangement levels were also observed in the *Tw*$^{+}$ and *Sod2*$^{+/-}$;*Tw*$^{+}$ mice. (*D*) Sequence coverage in *Sod2*$^{+/-}$ 1 correlates with H-strand G content but not with total G+C content. The skew is calculated as (C−G)/(C+G) in a 251-bp analytical window. The L-strand C content is the same as the H-strand G content.

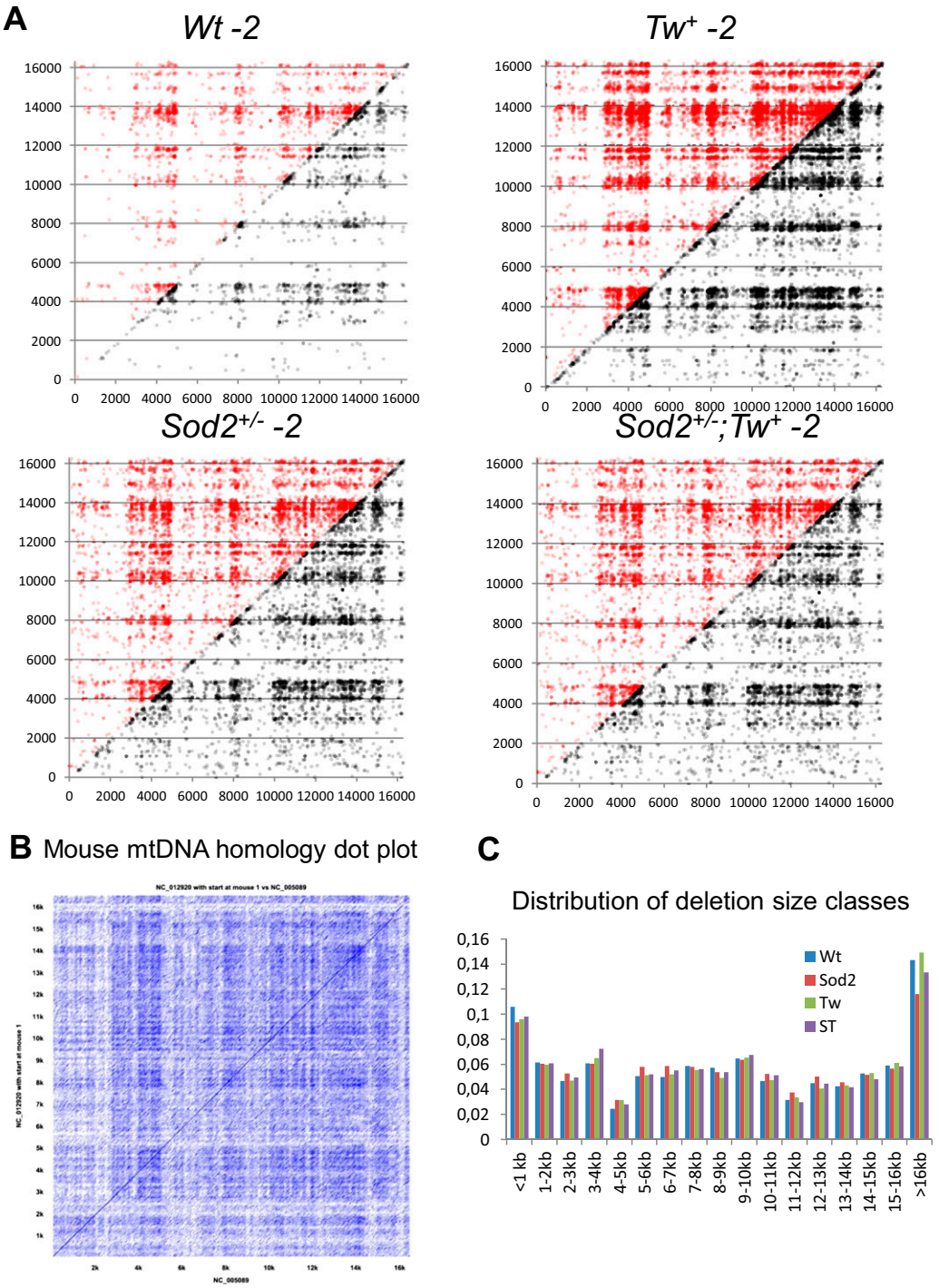

Fig. S3. Breakpoints of rearranged molecules correspond to homologous sequences on mouse mtDNA. (*A*) 3′- and 5′-breakpoints of rearranged mtDNAs from mice not included in Fig. 3. Breakpoint patterns correspond to homologous sequences revealed by plotting mouse mtDNA sequence against itself (*B*). (*C*) Approximately 14% of 3′- and 5′-breakpoint positions are located within a 300-bp distance based on breakpoint locations.

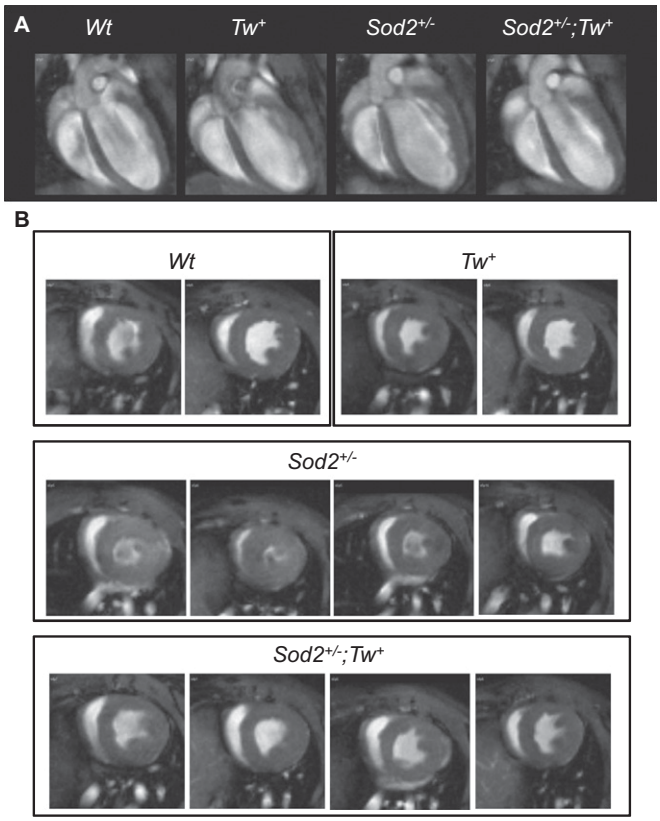

Fig. S4. Examples of the mouse heart phenotypes assessed by MRI. (*A*) Coronal plane views of hearts during end-diastolic phase. Note the altered shape of *Sod2*$^{+/-}$ mouse hearts. (*B*) Transverse plane views at the level of papillary muscle during end-systolic phase. *Tw*$^{+}$ mice are comparable with *Wt* mice, but *Sod2*$^{+/-}$ mouse hearts display increased ventricular wall thickness. Please also note individual variations in the degree of cardiomyopathy. The phenotype is markedly improved in *Sod2*$^{+/-}$/*Tw*$^{+}$ mice.

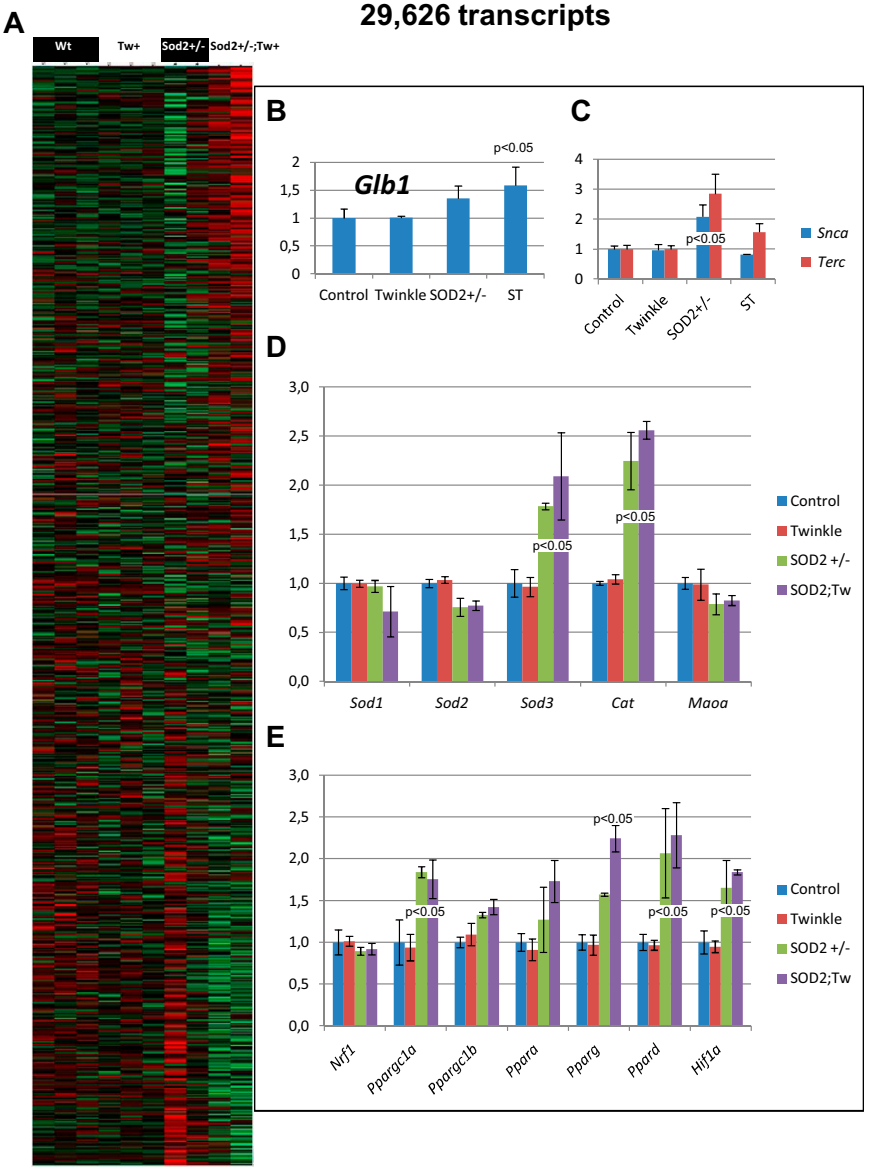

Fig. S5. (Continued)

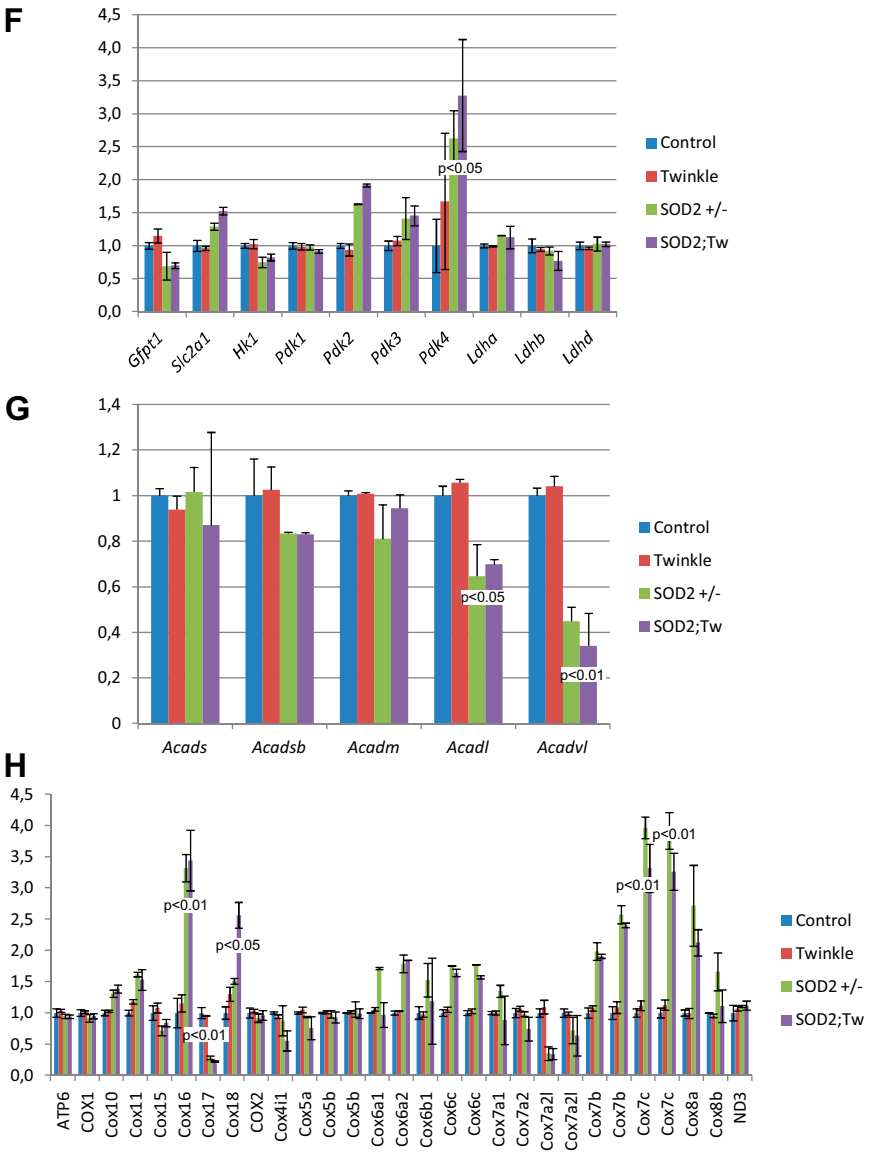

Fig. S5. Examples of expressional changes in Tw^{+} and $Sod2^{+/-}$ mice. (*A*) Heat-map clustering of heart samples based on expression levels of 29,626 genes. *Wt*, Tw^{+}, $Sod2^{+/-}$, and $Sod2^{+/-}$;Tw^{+} are separated in distinct clusters. Major changes in the expression pattern are evident in $Sod2^{+/-}$ and $Sod2^{+/-}$;Tw^{+} mouse hearts. (*B*) $Sod2^{+/-}$ and $Sod2^{+/-}$;Tw^{+} hearts show elevated levels of senescence associated β-galactosidase, *Glb1*. (*C*) α-Synuclein (*Snca*) and the RNA component of telomerase (*Terc*) are among the few differentially regulated genes in $Sod2^{+/-}$ and $Sod2^{+/-}$;Tw^{+} mouse. (*D*) $Sod2^{+/-}$ mice compensate the loss of *Sod2* allele by up-regulation of *Sod3* and catalase (*Cat*) and by down-regulation of the ROS-producing monamine oxidase (*Maoa*). (*E*) $Sod2^{+/-}$ and $Sod2^{+/-}$;Tw^{+} mouse hearts show increased expression of factors involved in mitochondrial biogenesis, namely PGC-1α (*Ppargc1a*), PPARs, and HIF-1α, which is likely related to activation of mTOR signaling. (*F*) Down-regulation of Glucosamine-fructose-6-phosphate aminotransferase (*Gfpt1*), increase of the main glucose transporter (*Glut1* or *Slc2a1*) and pyruvate dehydrogenase kinases (*Pdk2-4*) indicate increased glucose dependency of $Sod2^{+/-}$ mouse hearts. The latter enzymes are negative regulators of the mitochondrial OXPHOS inhibiting pyruvate dehydrogenase. (*G*) The key enzymes of beta oxidation of fatty acids are down-regulated in $Sod2^{+/-}$ mouse hearts as a response to increased glucose dependency. (*H*) Examples of genes involved in electron transport chain function. Differential regulation between $Sod2^{+/-}$ and $Sod2^{+/-}$;Tw^{+} was only observed for *Cox18* and *Cox8b*. Expression of mitochondria-encoded genes, such as *ATP6*, *COX1*, and *ND3*, was similar in all animals. Transcriptome data are available via ArrayExpress Archive as indicated in *Materials and Methods*. All *P* values were calculated by one-way ANOVA with Tukey's multiple comparison test.

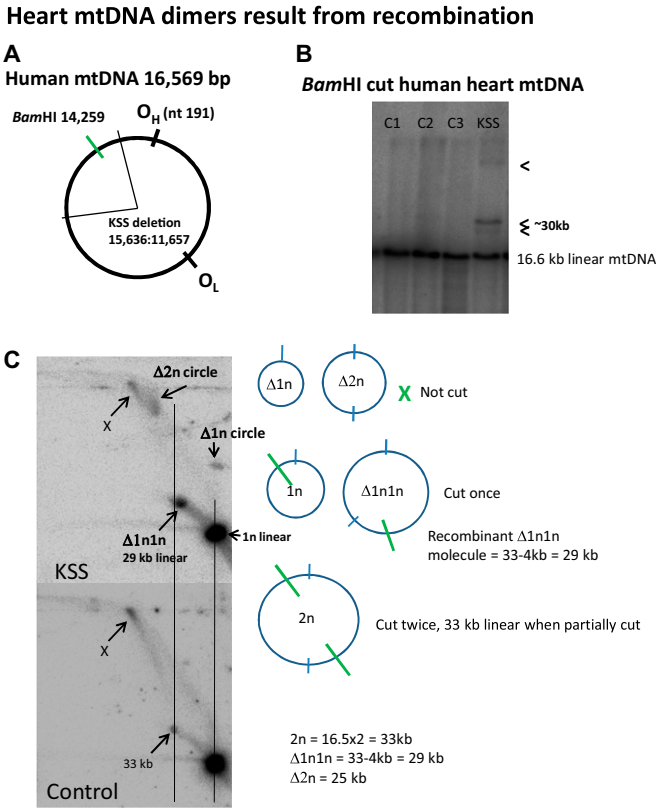

Fig. S6. Recombinant mtDNA in human heart. (*A*) The common 4-kb deletion in KSS removes the single BamHI restriction site on human mtDNA. (*B*) A Southern blot BamHI cut mtDNA from healthy control (C1-C2) and KSS patient. Open arrowheads indicate a number of bands bigger than the 16.6-kb linear mtDNA. Notice the strong band at approximately 30 kb. (*C*) A more detailed analysis of the rearranged mtDNA forms from KSS patient using 2D-AGE reveals unicircular deletion dimers (Δ2n) and recombinant Δ1n1n molecules, resulting in a 29-kb linear molecule when cut by BamHI.

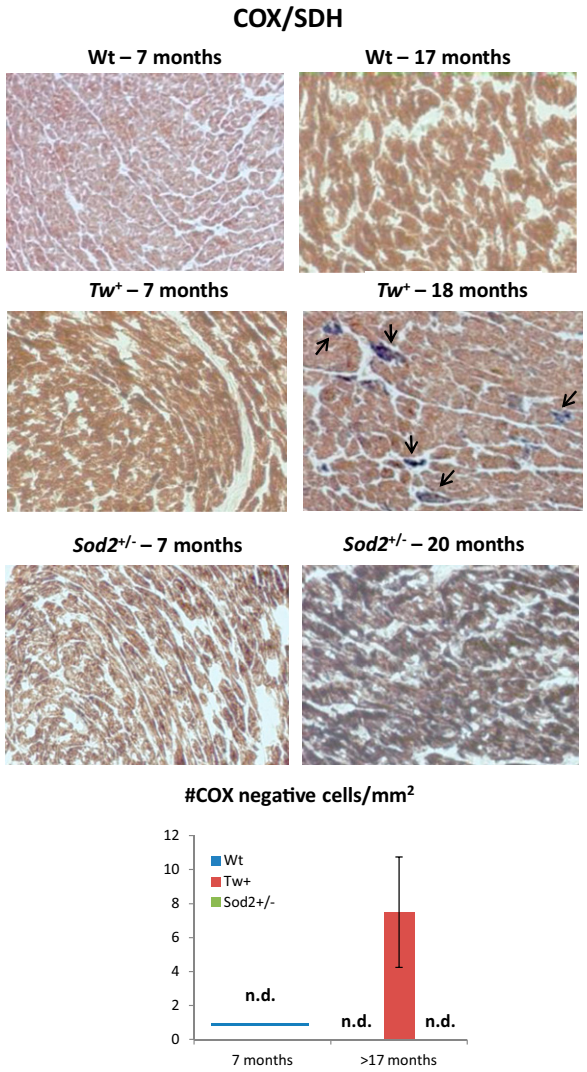

Fig. S7. COX-negative cardiomyocytes in aged Tw^{+} hearts. Cytochrome oxidase-deficient cardiomyocytes are stained blue by the SDH counter stain (arrows). Aged $Sod2^{+/-}$ hearts show SDH hyperactivity as indicated by the stronger bluish hue but no increase of individual COX-negative cells.